Int. J. Electrochem. Sci., 13 **(2018)** 5630 – 5644, doi: 10.20964/2018.06.16

International Journal of ELECTROCHEMICAL SCIENCE
www.electrochemsci.org

Impact of Li_2O/Metal Mole Ratio on Lithium-ion Battery Anode Performance

Muharrem Kunduraci[1,*], *Turkan Gamze Ulusoy Ghobadi*[2,3], *Eda Yilmaz*[2]

[1] Department of Mechanical Engineering, Faculty of Engineering, University of Turkish Aeronautical Association, Ankara 06790, Turkey
[2] UNAM – National Nanotechnology Research Center and Institute of Materials Science and Nanotechnology, Bilkent University, Ankara 06800, Turkey
[3] Department of Energy Engineering, Faculty of Engineering, Ankara University, Ankara 06830, Turkey
[*]E-mail: kunduraci.m@hotmail.com

Received: 23 January 2018 / *Accepted:* 23 March 2018 / *Published:* 10 May 2018

In this study the electrochemical impact of Li_2O/metal mole ratio on the cycle life of lithium-ion battery anode materials is demonstrated. For this purpose, nanostructured layered $LiNi_{1/3}Mn_{1/3}Co_{1/3}O_2$ (LiNMC) and spinel $LiMn_{1.5}Ni_{0.5}O_4$ (LiMNO) materials, traditionally known as cathode materials, are evaluated as anode materials and compared against their lithium-free versions NMC (Ni:Mn:Co=1:1:1) and MNO (Mn:Ni=3:1). The Li_2O/metal ratio in fully lithiated states are 2.0 for lithium containing (LiNMC and LiMNO) and 1.3 for lithium-free (NMC and MNO) samples. Battery tests show that capacity fading of lithium containing samples is 3 to 4 times larger than lithium-free samples. The differences in the electronic conductivities and voltages profiles of lithium containing and lithium-free anode materials are suggested to be the origin of such electrochemical disparity.

Keywords: lithium battery, conversion anode, composite,

1. INTRODUCTION

Since their publication in 2000 by Tarascon [1], the popularity of transition metal oxides as alternative anodes to graphite in lithium-ion batteries have grown steadily. NiO [2], Co_3O_4 [3], ZnO [4], MnO [5] are some of the transition metal oxides that have been widely studied due to their low cost and easy synthesis. Regardless of the metal utilized, or whether the oxide consists of a single phase or has a nanocomposite structure, metal nanoparticles (MNP) dispersed within a Li_2O matrix in fully discharged (i.e. lithiated) state is the common denominator in all transition metal oxide anodes.

From this perspective, the structure in discharged state is actually a composite material. We know from materials science that the physical properties of composite materials such as strength and ductility are highly dependent on the type, size, shape and volume fraction of dispersed phase or filler material. If we use a similar analogy here, the conversion efficiency of metal oxides should be dependent on the type of metal used, the size of metal nanoparticles at the end of discharge step and the mole ratios of Li_2O host and MNP filler materials. Just to demonstrate the idea about the last item, this ratio can range from 0.5 for Cu_2O, 1.0 for NiO, 1.33 for Co_3O_4 to 3.0 for MoO_3 as summarized below.

$$Cu_2O + 2Li \rightarrow 2Cu + Li_2O \quad (1)$$

$$NiO + 2Li \rightarrow Ni + Li_2O \quad (2)$$

$$Co_3O_4 + 8Li \rightarrow 3Co + 4Li_2O \quad (3)$$

$$MoO_3 + 6Li \rightarrow Mo + 3Li_2O \quad (4)$$

In this work, we demonstrate the significance of Li_2O/metal mole ratio at the end of full lithiation on the capacity retention of anode material. To the best of our knowledge, this is the first time this has been attempted. However, we should acknowledge the work by Gu [6] who synthesized MnO_x anode materials with varying average manganese valency. Among the MnO_2, Mn_2O_3, Mn_3O_4 and MnO that were synthesized, MnO seems to have the best performance in our opinion. The authors did not put out any argument about the Li_2O/metal mole ratio

In this work, we synthesized layered $LiNi^{2+}_{1/3}Mn^{4+}_{1/3}Co^{3+}_{1/3}O_2$ (LiNMC) and spinel $LiMn^{4+}_{1.5}Ni^{2+}_{0.5}O_4$ (LiMNO), which are commonly used as cathode materials in literature [7-10]. They were evaluated as anode materials and compared against their lithium-free counterparts with the same transition metal ratios NMC (Ni:Mn:Co=1:1:1) and MNO (Mn:Ni=3:1), respectively. Our results show a much faster capacity fading for LiNMC and LiMNO anode materials than their lithium-free counterparts.

2. EXPERIMENTAL

2.1. Material Synthesis

The anode materials $LiNi^{2+}_{1/3}Mn^{4+}_{1/3}Co^{3+}_{1/3}O_2$ (LiNMC), $LiMn^{4+}_{1.5}Ni^{2+}_{0.5}O_4$ (LiMNO) and their lithium-free versions with the same transition metal ratios NMC and MNO were synthesized by Pechini process. The details of the process are provided elsewhere [11]. This process was chosen because of its ability to enable atomic scale mixing of multiple elements. At the end of wet synthesis step, the anode materials were ground and initially heated to 450 ^oC for 1 h in air to burn the organic residues. Following the first heating step, LiNMC and NMC were later heated to 800 ^oC for 10 h in air to obtain crystalline structures. On the other hand, LiMNO and MNO were heated to 700 ^oC for 10 h in air as this temperature was known to be high enough to obtain well crystallized materials.

2.2. Materials Characterization

The morphological characteristics of the synthesized anode materials were performed using scanning electron microscope (SEM, FEI – Quanta 200 FEG) operated at 10 kV. Energy-dispersive X-

ray spectroscopy (EDX) analysis was also performed for elemental analysis. Powder X-ray diffraction (PXRD) has been carried out by Panalytical X'pert Multi-Purpose and the patterns have been collected in the range of 2θ = 20–80° using Bragg–Brentano geometry (Cu Kα radiation, λ= 0.15418 nm). X-ray photoelectron spectroscopy (XPS, Thermoscientic K-Alpha, Al K-Alpha radiation, hυ = 1486.6 eV) measurements were performed at survey mode by operating flood gun to prevent surface charging with the pass energy and step size set to 30 eV and 0.1 eV, respectively. Peak position correction was calibrated by referencing the C1s peak position (284.8 eV) and shifting other peaks in the spectrum accordingly. For oxidation state determination; depth profiling was carried out by using XPS with Ar+ ions having energy of 1000 eV. The depth profiles of the samples were generated in 10 cycles, each XPS spectrum collected after exposing the sample to the gas cluster ion beam for 200 s.

2.3. Electrochemical Characterization

The anode slurries were prepared by first dissolving Polyvinylidene fluoride (PVDF) binder in N-methyl-2-pyrrolidone solvent. After the clear solution was obtained, conductive agent Super P followed by anode active material (LiNMC, NMC, LiMNO or MNO) were added to the PVDF/NMP solution. The slurry was stirred for overnight at 500 rpm. The slurry consisted of 70 wt% anode material, 15 wt% PVDF and the remaining 15 wt% conductive carbon material in cases of LiNMC and NMC anodes. The formulation was 50:25:25 wt%, respectively for LiMNO and MNO. The electrode materials were vacuum dried at 70 °C overnight, then rapidly put into argon filled glovebox (O2 <0.5 ppm, H_2O <0.5 ppm) to prevent air exposure. Swagelok type cells were used to build lithium half cells. Celgard C480 separators were utilized at anode while separators of the cathodes were glass microfiber filter (GF/C). The electrolyte solutions of the cells were composed of 280 µL of 1 M LiTFSI dissolved in EC:DMC (1:1) solution. The cells were sealed after the assembly to prevent interaction with the atmosphere, and rested at room temperature for 8 hours prior to testing. Electrochemical tests were conducted with Landt CT2001 multichannel potentiostat/ galvanostat at 100 mA/g current rate between 0.2 V and 3 V potential window. The active anode mass ranged from 1.1 mg to 2.6 mg. The AC impedance spectroscopy analysis was carried out at the end of first charge (delithiation) step by applying 5 mV alternating voltage. The frequency range was from 1 kHz to 0.01 Hz. The impedance data were normalized with respect to the active material amount in coin cells.

3. RESULTS AND DISCUSSION

SEM analyses were carried out to investigate the particle size and morphology of the anode materials. All samples consist of primary particles with 100-200 nm in diameter (Figure 1.a-d). These particles seem to be interconnected with nanosized pores between them. This morphology was recorded previously [11]. The presence of nanoparticles is believed to be conducive to the reversibility of anode materials [12-14]. In order to ascertain whether the atomic ratios of transition metals in the synthesized materials are in accordance with the numbers intended prior to the synthesis, EDX

elemental analysis was carried out. The elemental mole ratios of Ni, Mn and Co atoms are provided in Table 1. The deviation from the intended compositions is less than 3%, thereby being in excellent agreement with desired values.

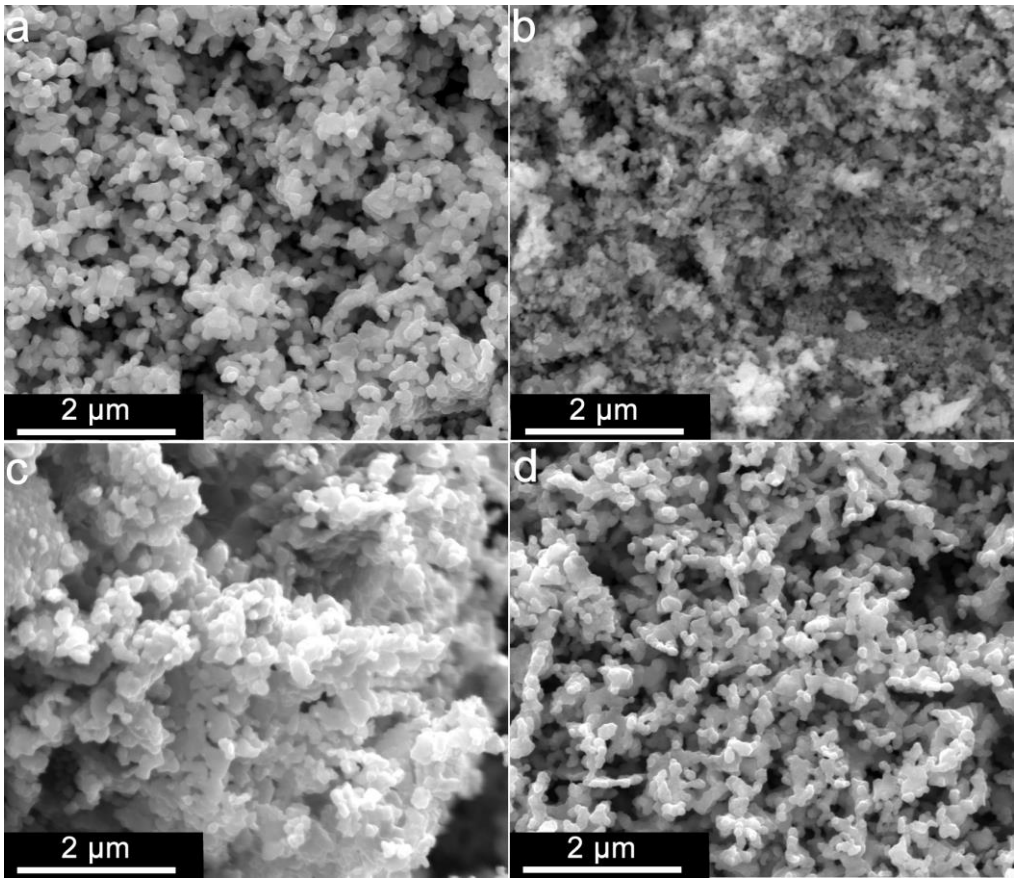

Figure 1. Scanning electron microscopy images of nanostructured a) LiNMC b) NMC c) LiMNO and d) MNO materials

Table 1. Summary of X-ray diffraction phase analyses and SEM-EDS elemental analyses of four anode materials

	XRD phase analysis	Phase Description	SEM-EDX elemental analysis					
			Ni	Mn	Co	Ni	Mn (normalized)	Co
LiNMC	single phase $LiNi_{1/3}Mn_{1/3}Co_{1/3}O_2$	($LiMO_2$ layered)	18.19	18.94	19.09	0.32	0.34	0.34
NMC	$0.15NiO + 0.85(Ni,Mn)(Co,Mn)_2O_4$	(rock salt + AB_2O_4 spinel)	24.45	22.97	23.47	0.35	0.32	0.33
LiMNO	single phase $LiMn_{1.5}Ni_{0.5}O_4$	($Li_2A_3BO_8$ spinel)	14.46	41.18	-	0.52	1.48	-
MNO	single phase $(Ni_{0.75}Mn_{0.25})Mn_2O_4$	(AB_2O_4 spinel)	16.12	48.83	-	0.50	1.50	-

The phase analyses of the samples were performed by X-ray diffraction. The diffraction spectra of all four samples are provided in Figure 2. The samples LiNMC, LiMNO and MNO were found to contain single phase only with no sign of any secondary phase. LiNMC diffraction peaks were assigned to layered type $LiNi_{1/3}Mn_{1/3}Co_{1/3}O_2$ phase (PDF no: 98-016-3314). LiMNO is a single phase Fd3m type spinel material with the formulation of $LiMn_{1.5}Ni_{0.5}O_4$ (PDF no: 98-007-0023). The closest

match to MNO material in the database was $NiMn_2O_4$ spinel material with PDF number 98-018-1111. However, we know that Mn-to-Ni ratio in our material is 3-to-1. Therefore, the actual composition of MNO is corrected as $(Ni_{0.75}Mn_{0.25})Mn_2O_4$ which is a AB_2O_4 type spinel structure. For sample NMC, a primary phase of AB_2O_4 type spinel and a small amount (15%) of rock salt type NiO phase were identified. While an exact assignment of metals for each position is challenging due to the ternary nature of the NMC sample, we think that A site is mostly occupied by nickel atoms and cobalt atoms occupy exclusively B site with manganese atoms distributed over both sites.

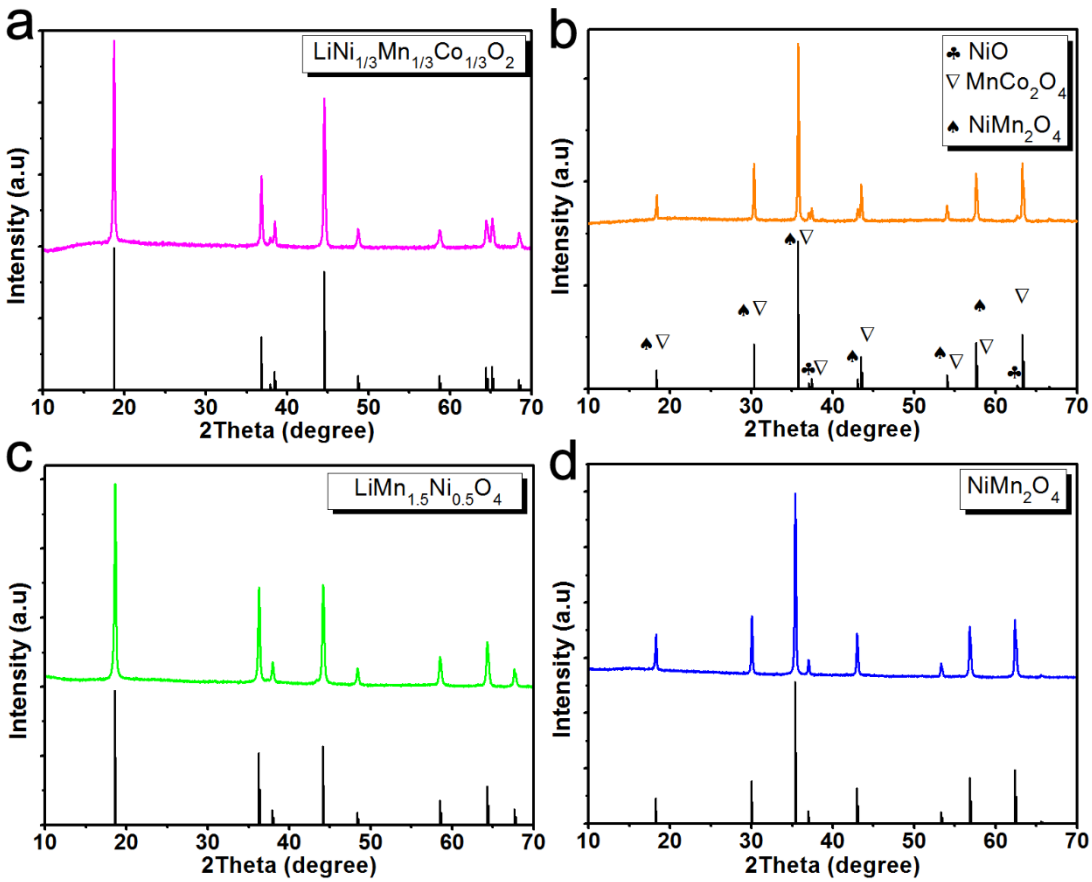

Figure 2. X-ray diffraction spectra a) LiNMC ($LiNi_{1/3}Mn_{1/3}Co_{1/3}O_2$) b) NMC [$NiO+(Ni,Mn,Co)_3O_4$] c) LiMNO ($LiMn_{1.5}Ni_{0.5}O_4$) and d) MNO ($Ni_{0.75}Mn_{2.25}O_4$) materials

In order to determine the oxidation states of transition metals in anode materials, XPS (x-ray photoelectron spectroscopy) spectra of all four samples were taken after synthesis (Figure 3). The determination of the oxidation states of transition metals was based on the deconvolution of their $2p^{3/2}$ peaks as well as the location of the constituent peaks. In $LiNi_{1/3}Mn_{1/3}Co_{1/3}O_2$, Mn $2p^{3/2}$, Co $2p^{3/2}$ and Ni $2p^{3/2}$ peaks were centered around 642-642.5 eV, 780.4 eV and 855 eV, respectively (Figure 3.a-c) consistent with earlier reports [15]. Therefore, we concluded that the only ions present in LiNMC are Mn^{4+}, Co^{3+} and Ni^{2+}. In Figure 3.g-h, The Mn $2p^{3/2}$ and Ni $2p^{3/2}$ peaks are provided for $LiMn_{1.5}Ni_{0.5}O_4$. They are located around 641.8-642.5 eV and 854 eV, respectively and were attributed to Mn^{4+} and Ni^{2+} previously [16-17]. Spinel $(Ni_{0.75}Mn_{0.25})Mn_2O_4$ was reported to be partially inversed in which Ni^{2+} occupy the octahedral sites. Also, due to the instability of Mn^{3+} ions because of Jahn-Teller effect,

manganese ions adopt mixed oxidation states having +2, +3 and +4 valencies [18]. The best fitting of manganese spectra was achieved when we assumed all three manganese oxidation states co-exist. The Mn^{2+}, Mn^{3+} and Mn^{4+} peaks are available in Figure 3.i and are consistent with earlier reports [19-20]. Based on the composition of $(Ni_{0.75}Mn_{0.25})Mn_2O_4$ anode material as well as the XPS spectra results, average oxidation state of manganese ions was calculated to be ~2.89 for MNO.

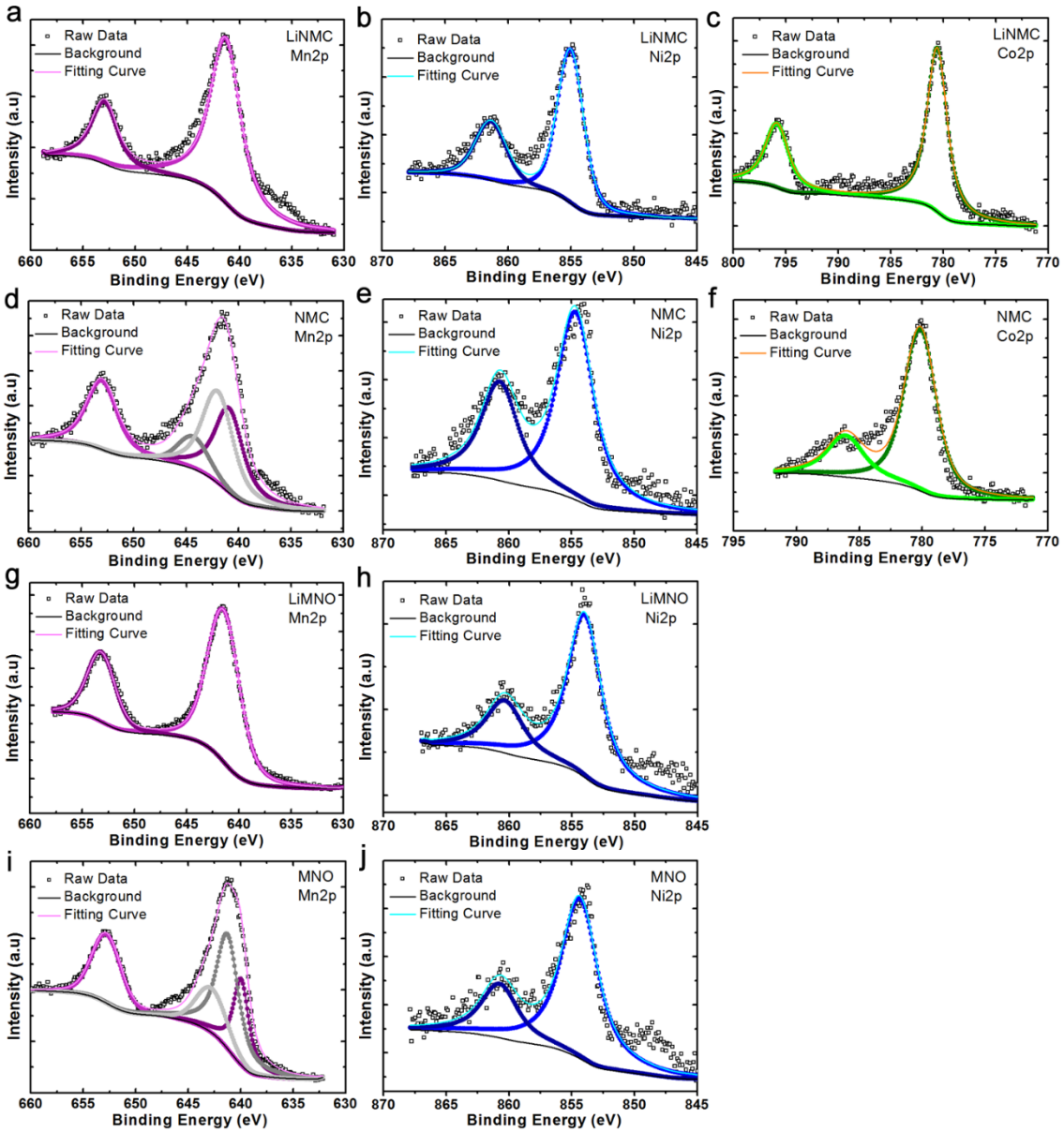

Figure 3. X-ray photoelectron spectroscopy Mn $2p^{3/2}$ Ni $2p^{3/2}$ and Co $2p^{3/2}$ peaks of fresh LiNMC (a-c), NMC (d-f), LiMNO (g-h) and MNO (i-j) materials

Finally, the XPS spectrum of Mn, Ni and Co in NMC are given in Figure 3.d-f. Similar to other materials, cobalt and nickel elements are found to exist as 3+ and 2+ ions, respectively. On the other hand, manganese ions are believed to have 2+, 3+ and 4+ oxidation states. The average oxidation state of manganese in NMC was calculated to be ~2.90 similar to the one in MNO.

A significant point needs to be made clear before further continuing with electrochemical testing results. The assignment of lattice positions and oxidation states of metal ions were done judicially for all four materials based on XRD and XPS results as well as available literature. While the task was quite straightforward for LiNMC and LiMNO, the oxidation states of manganese ions as well as their distribution over two lattice sites cannot be exact for NMC and MNO. However, since all materials disintegrate into metal nanoparticles dispersed in a Li_2O matrix upon discharging, the Li_2O/metal ratio in the final structure will be same whether the fresh anode material has two Mn^{3+} ions or one of each Mn^{2+} and Mn^{4+} ions. However, we cannot comment on the impact this will have on the size of nano metal grains at discharged state.

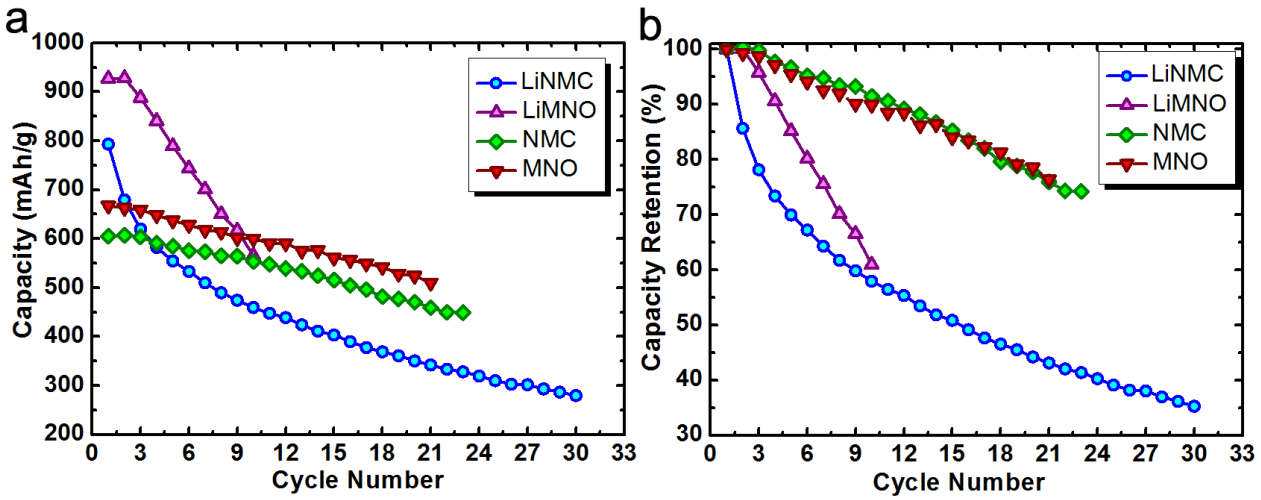

Figure 4. a) Charge capacity (mAh/g) and b) percent capacity retention values of four anode materials as a function of cycle number

The electrochemical impact of Li_2O/metal mole ratio in the fully discharged state was studied by evaluating the charge-discharge behaviors of LiNMC and NMC anode materials. Their charge capacities at different cycle numbers are given in Figure 4.a. The first cycle discharge (lithiation) capacities of LiNMC and NMC are 1027 and 993 mAh/g, respectively.

Table 2. First cycle lithiation mechanism of four anode materials with final Li_2O/metal ratios in fully lithiated states

$LiNi^{2+}_{1/3}Mn^{4+}_{1/3}Co^{3+}_{1/3}O_2 + 3Li^+ + 3e^- \rightarrow 1/3(Ni^0 + Mn^0 + Co^0) + 2Li_2O$	(Li_2O/M=2)
$0.15Ni^{2+}O + 0.85[Ni^{2+}_{0.9}Co^{3+}_{1.05}Mn^{2.90+}_{1.05}]O_4 + 7.1Li^+ + 7.1e^- \rightarrow \sim 0.90(Ni^0 + Mn^0 + Co^0) + 3.55Li_2O$	(Li_2O/M=1.31)
$LiMn^{4+}_{1.5}Ni^{2+}_{0.5}O_4 + 7Li^+ + 7e^- \rightarrow 1.5Mn^0 + 0.5Ni^0 + 4Li_2O$	(Li_2O/M=2)
$Ni^{2+}_{0.75}Mn^{2.89+}_{2.25}O_4 + 8Li^+ + 8e^- \rightarrow 2.25Mn^0 + 0.75Ni^0 + 4Li_2O$	(Li_2O/M=1.33)

The theoretical discharge capacities of the same materials based on the discharge mechanism given in Table 2 are calculated as 841 mAh/g and 875 mAh/g, respectively. The extra capacity from

interfacial storage was excluded in the calculation of theoretical capacities [21]. Based on the ratios of theoretical and actual discharge capacities, it can be concluded that both anode materials perform similarly. The 10-20% extra capacities above the theoretical values should stem from charge loss to SEI formation as well as possible interfacial lithium storage. Despite similar discharge behavior, a very noticeable difference is observed in charge (delithiation) capacities. The LiNMC has a 1st cycle charge capacity of 793 mAh/g while NMC can only achieve 605 mAh/g (delithiation capacities of similar materials from literature are provided for comparison in Table 3 in supporting information). These numbers correspond to about 77% and 61% coulombic efficiencies for LiNMC and NMC anode materials, respectively (Figure S1). These results were confirmed with sister cells. Given that both anode electrodes had the same formulation, such a disparity between two anode materials with the same metal composition might be explained by the difference in average metal nanoparticle diameters in their fully lithiated states as well as the availability of extra Li_2O matrix in LiNMC.

Looking at the charge and discharge reactions in Table 2 for LiNMC and NMC anode materials, we can notice that Li_2O/metal mole ratio is 2.0 for LiNMC and 1.3 for NMC in their fully discharged states. The volume fraction of metal nanoparticles in fully discharged state can be approximated using equation 1 given below.

Equation 1.

$$vol\%\ of\ M = \frac{C}{1+C}\ , \qquad C = \frac{\rho_{Li2O} * AW_M}{\left(\frac{Li_2O}{M}\right) * \rho_M * MW_{Li2O}}$$

where ρ_{Li2O}=2.01 g/cc (density of Li_2O), ρ_M=8.90 g/cc (density of metal), AW_M=~58 g/mol (atomic weight of metal), MW_{Li2O}=29.9 g/mol (molecular weight of Li_2O) and (Li_2O/M) is the mole ratio of Li_2O to metal nanoparticles at the end of discharged state.

Using the above equation, the volume fraction of metal nanoparticles is calculated to be 18% for LiNMC and 25% for NMC materials. While an undisputable conclusion cannot be drawn from these numbers alone, we think that the average diameter of metal nanoparticles in fully discharged state is smaller in case of LiNMC. This is a reasonable speculation as metal nanoparticles would be more diluted inside Li_2O matrix and end up with a smaller size with LiNMC anode material. Since the oxidation conversion reaction in charging step takes place at the Li_2O/metal interface, smaller metal particles are expected to have better reversibility, thereby explaining larger coulombic efficiency for LiNMC than NMC. Besides the size effect, it can be reasoned that the extra amount of Li_2O (about 50% more) in the case of LiNMC will make it easier for transition metal atoms to get oxidized during charging step.

However, upon further cycling a much faster capacity decay is observed with LiNMC anode material than its lithium-free counterpart (Figure 4.b). The rate of loss in charge capacity in the first 10 cycles of LiNMC is about 37 mAh/g per cycle, corresponding to 4.6% loss. On the other hand, the loss in NMC is much lower, namely 5.7 mAh/g or 0.9% per cycle. In order to make sure that such behavior can be repeated with other anode chemistries and electrode formulations, we synthesized LiMNO ($LiMn^{4+}_{1.5}Ni^{2+}_{0.5}O_4$) and its lithium-free version MNO ($Ni^{2+}_{0.75}Mn^{2.89+}_{2.25}O_4$) and compared their electrochemical performance as anode materials. The electrode formulation was changed to 50-25-25 where conductive carbon additive is 25wt% as opposed to 15wt% in cases of LiNMC and NMC. This

was done with the intention to mitigate the thoughts about the role of electrode's electronic conductivity.

The discharge mechanisms of LiMNO and MNO are provided in Table 2. Similar to LiNMC and NMC anodes, in the fully discharged state Li_2O/metal mole ratio is 2.0 and 1.33 for LiMNO and MNO, respectively. Therefore, as far as Li_2O/metal mole ratio is concerned, LiNMC and LiMNO are equals just as NMC and MNO are. The charge capacities as well as percent capacity retentions of LiMNO and MNO anode materials as a function of cycle number are plotted in Figure 4.a-b. We can see that LiMNO and MNO couple behave just like LiNMC and NMC couple. The capacity loss rate is 40.2 mAh/g for LiMNO and 7.5 mAh/g for MNO, corresponding to 4.3% and 1% loss per cycle. The first cycle coulombic efficiency is 72% for $LiMn^{4+}_{1.5}Ni^{2+}_{0.5}O_4$ and 60% for $Ni^{2+}_{0.75}Mn^{2.89+}_{2.25}O_4$. The larger number for LiMNO suggests that it is the one with smaller metal nanoparticles just like the case with LNMC and NMC anode materials. However, both numbers are smaller than those of LiNMC and NMC. The reason might lie in the binary vs. ternary nature of both systems. From materials science perspective the presence of more metals would hinder the growth of metal nuclei. Therefore, it can be speculated that the ternary LiNMC anode material has higher first cycle coulombic efficiency than its binary LiMNO counterpart because the former has smaller diameter metal nanoparticles in discharged state. With that said, we cannot rule out the possibility that cobalt atoms have a better reversiblity than both manganese and nickel atoms.

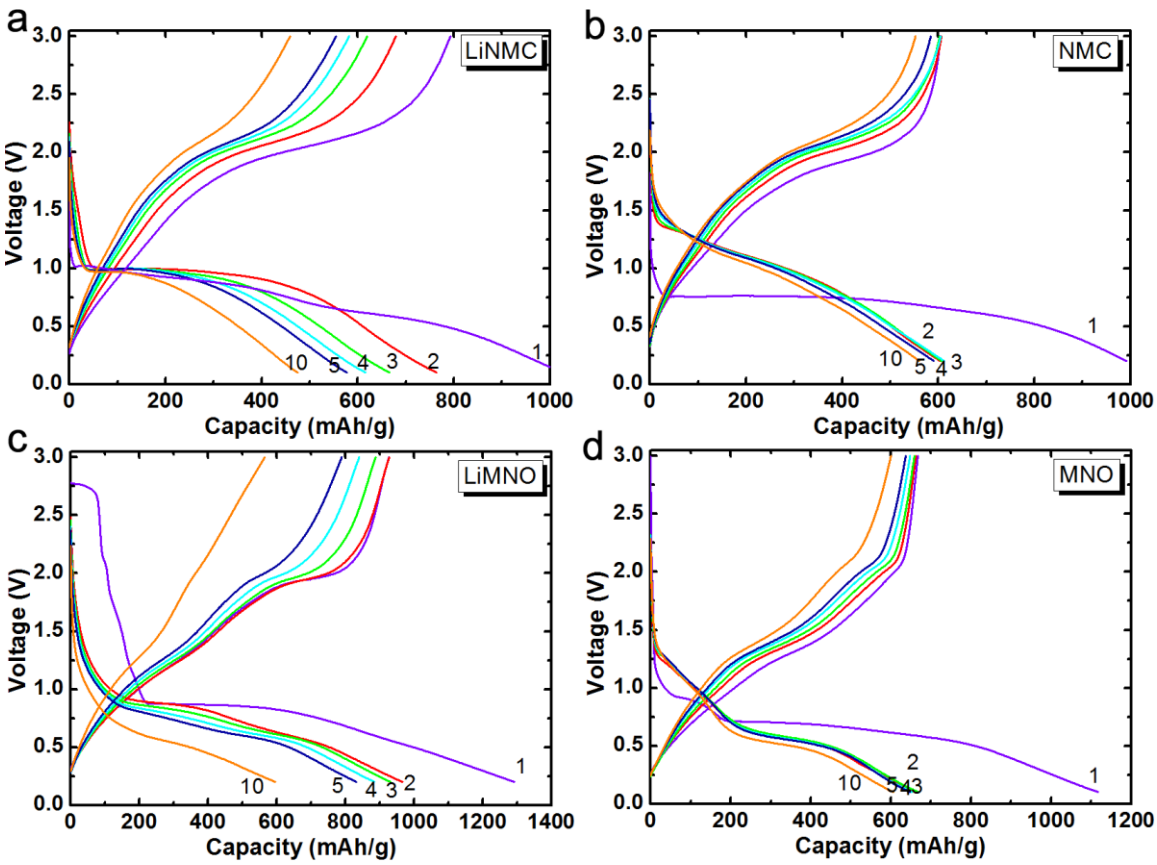

Figure 5. Charge-discharge voltage profiles of four anode materials as a function of cycle number

In order to explain the difference in the capacity fading rates of Li-rich and Li-free anode materials, their charge and discharge voltage profiles were examined. In Figure 5.a-d, 1st, 2nd, 3rd, 4th, 5th and 10th cycle voltage profiles are shown. A clear difference in the discharge profiles of LiNMC and NMC can be easily noticed in Figure 5.a and b. While there is a distinct and wide,plateau at 1.0 V in case of LiNMC anode material, the discharge voltage profile of NMC is rather sloping and lacks any distinctive character. Similarly but less noticeably, it can be argued that the voltage profiles of LiMNO are flatter than those of MNO anode material. These observations suggest that the mechanisms of lithiation and delithiatin processes are somewhat different for Li-rich (LiNMC and LiMNO) and Li-free (NMC and MNO) anode materials despite the same chemical compositions. Such a difference should stem from the distribution of transition metals within the matrix at the end of lithiation step. Whether Co, Mn and Ni atoms segregate into individual metallic grains or form binary or ternary grains would explain such anomaly. We think that this point deserves much investigation using advanced atomic probing techniques.

X-ray photoelectron spectroscopy studies were performed at the end of first charging (delithiation) step to reveal oxidation states of transition metals. The Mn $2p^{3/2}$ peak is centered around 641.5 eV in all materials as shown in Figure 6.a-d.

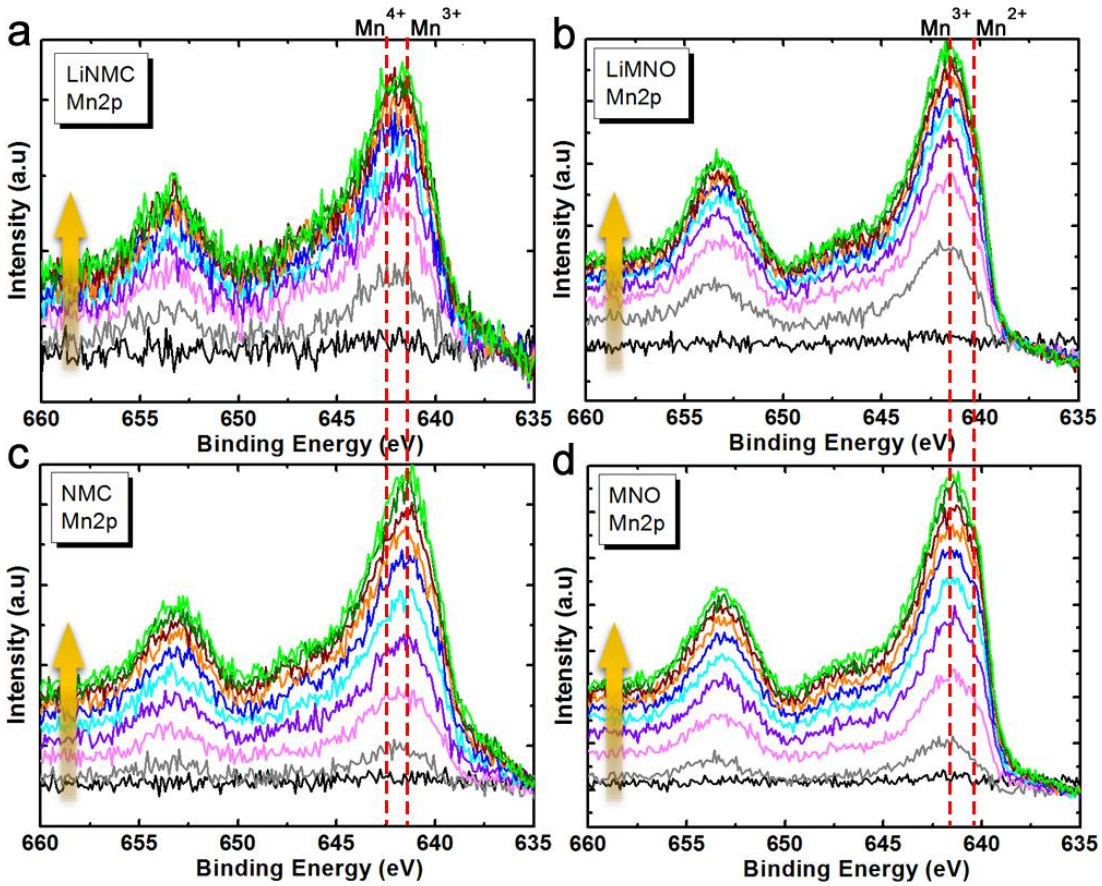

Figure 6. X-ray photoelectron spectroscopy Mn $2p^{3/2}$ peaks of four anode materials at the end of first delithiation step. Dashed lines were added to help guide eye. The arrows point the direction of etching (i.e. towards the bulk of the sample).

This peak has been assigned to Mn^{3+} previously [22]. However, small shoulders at 642.5 eV and 640.3 eV can also be noticed, corresponding to Mn^{4+} and Mn^{2+}, respectively. We concluded that manganese ions are oxidized to an average oxidation states of 3+ in all anode materials. As for cobalt ion, it seems to have 2+ and 3+ oxidation states in both LiNMC and NMC anode materials [23] as shown in Figure s2. Unlike manganese and cobalt ions which showed similar XPS spectrum for both Li-rich and Li-free anode material, we think that the distinction was more obvious with nickel ions. We can see a sharp peak located at 853 eV and a small peak on the right shoulder at 854 eV in cases of NMC and MNO anode material (Figure 7.c-d). These peaks have been assigned to Ni^0 and Ni^{2+}, respectively [24]. This result is in agreement with our previous work [25] that nickel atom has a smaller tendency for re-oxidation. We also noticed that the intensity of Ni^0 peak increases towards the core of the anode particle, suggesting poorer reversibility in the core of the anode material than at the center. On the other hand, Ni^0 peak is not as sharp in cases of LiNMC and LiMNO (Figure 7. a-b).

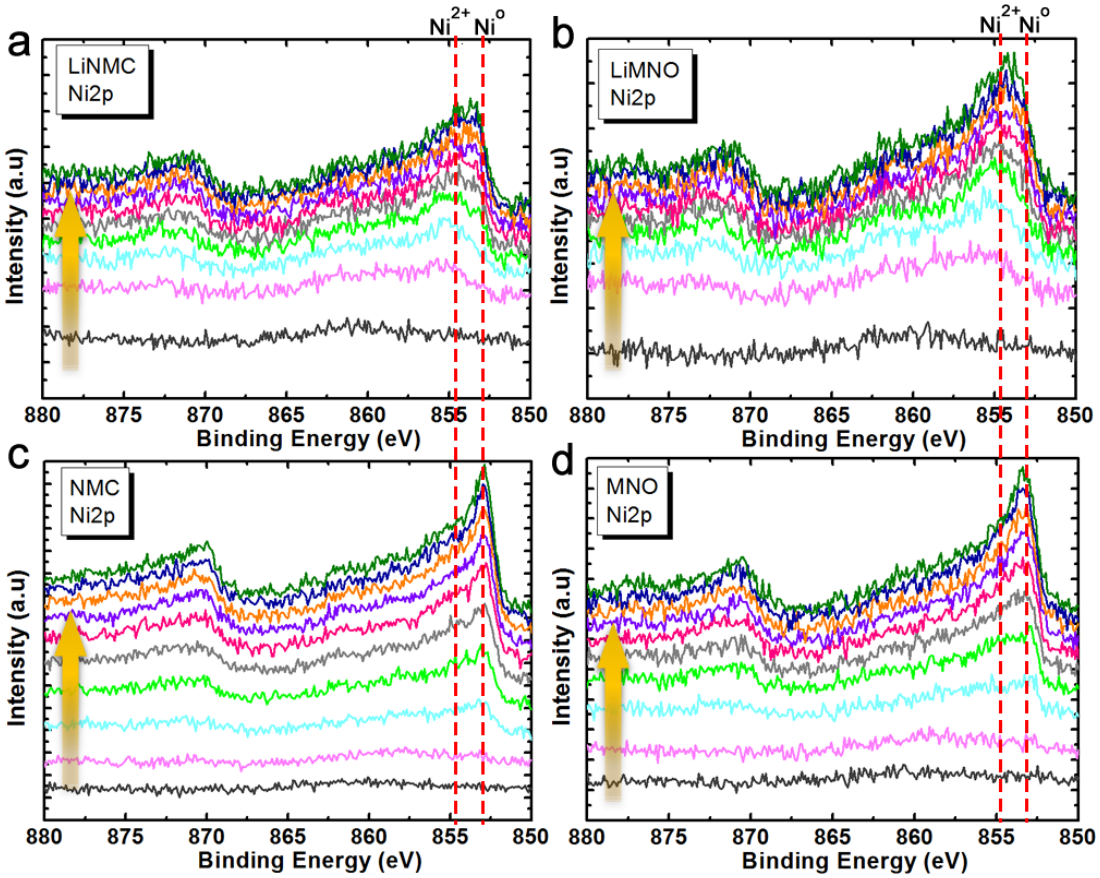

Figure 7. X-ray photoelectron spectroscopy Ni $2p^{3/2}$ peaks of four anode materials at the end of first delithiation step. Dashed lines were added to help guide eye. The arrows point the direction of etching (i.e. towards the bulk of the sample).

The higher oxidation state for nickel with LiNMC and LiMNO might be attributed to the availability of extra Li_2O matrix in these materials. While the lack of re-oxidation of nickel atoms to 2+ state is not favorable to the charge capacities of NMC and MNO anode materials, it helps with the

electronic conductivity of the very same anode materials. Therefore, we argue that the better cycle life of Li-free anode materials might be partially explained by their higher electronic conductivities.

Impedance spectroscopy analyses of anode materials were carried out to gain deepeer insights into the role of electronic conductivity. The spectra were collected at the end of first charging (delithiation) step for all samples. The Z-plot data of all four samples are provided in Figure 8. All four spectra have a high frequency arc which represents the charge transfer resistance (R_{ct}) followed by a low frequency Warburg slope. First thing to point out is that the charge transfer resistances of LiMNO and MNO couple are smaller than those of LiNMC and NMC couple. This might be explained by the larger amount of conductive carbon in the former couple. Secondly, in both couples lithium-free anode electrodes (i.e. NMC and MNO) have smaller R_{ct} than LiNMC and LiMNO electrodes. And finally, the slope of Warburg line is around 45^o for LiNMC and LiMNO while it is noticeable larger for NMC and MNO electrodes.

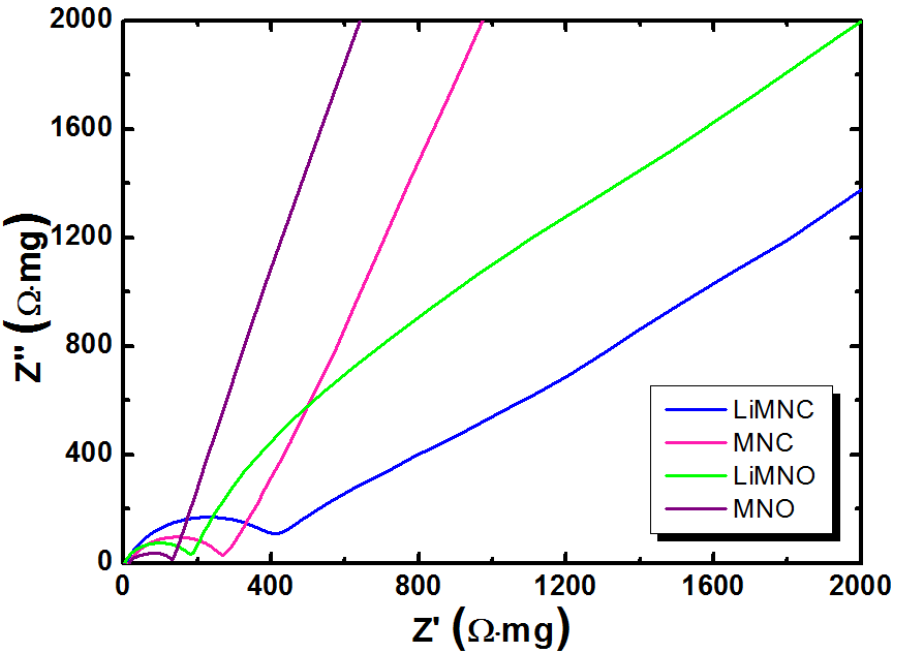

Figure 8. Z-plots of four anode materials at the end of first delithiation step.

The larger slope can be interpreted as more capacitive behavior. These two observations are consistent with the above argument that there are unoxidized nanosized metal grains in lithium-free anode materials at the end of charging step. These metallic nanograins increase the electronic conductivity and capacitive behavior of lithium-free anode materials, thereby helping charge transfer resistance and lithium capacity.

4. CONCLUSION

Nanostructured $LiNi_{1/3}Mn_{1/3}Co_{1/3}O_2$ (LiNMC) and $LiMn_{1.5}Ni_{0.5}O_4$ (LiMNO) as well as their lithium-free versions with the same transition metal ratios (NMC and MNO) were evaluated as battery

anode materials and compared against each other. Lithium-free NMC and MNO anode materials exhibited much smaller fading rates than LiNMC and LiMNO, thereby highlighting the positive impact of low Li_2O/metal mole ratio in fully lithiated state. We argued that two factors might be at play to explain the electrochemical disparity. Firstly, lithium-free NMC and MNO are suggested to have higher electronic conductivities than LiNMC and LiMNO due to the incomplete re-oxidation of nickel atoms in the former two anode materials. Secondly and probably more importantly, we think that upon initial lithiation the transition metal atoms take a distribution (i.e. chemical uniformity of nano metallic grains) in the final composite structure that is more favorable to cycle life in cases of NMC and MNO anode materials. The differences in the charge and discharge voltage profiles of lithium-rich and lithium-free anode materials suggest different pathways during lithiation and delithiation processes. We believe that these results can develop new interest in this area and advanced techniques that can probe at atomic scale can be utilized in the future for a complete understanding of this phenomena.

SUPPORTING INFORMATION

Table 3. List of some AB_2O_4 type anodes for lithium-ion batteries

Anode material	Delithiation capactity (mAh/g)	Current rate (mA/g)	Reference
$MnCo_2O_4$	910	200	[26]
$NiCo_2O_4$	750	500	[27]
$NiCo_2O_4$	950	100	[28]
$CoMn_2O_4$ (yolk-shell)	715	1000	[29]
$CoMn_2O_4$	721	200	[30]

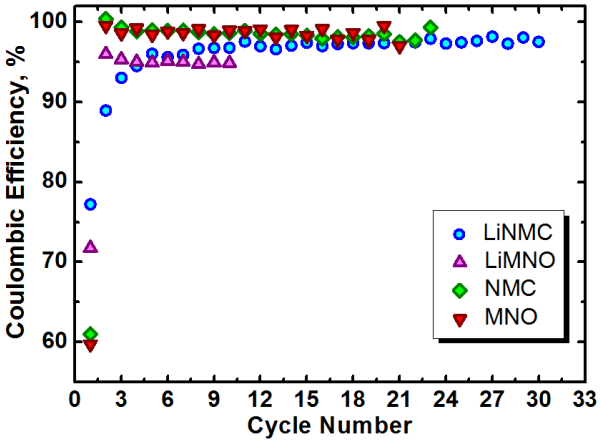

Figure S1. Coulombic efficiency of four anode materials as a function of cycle number

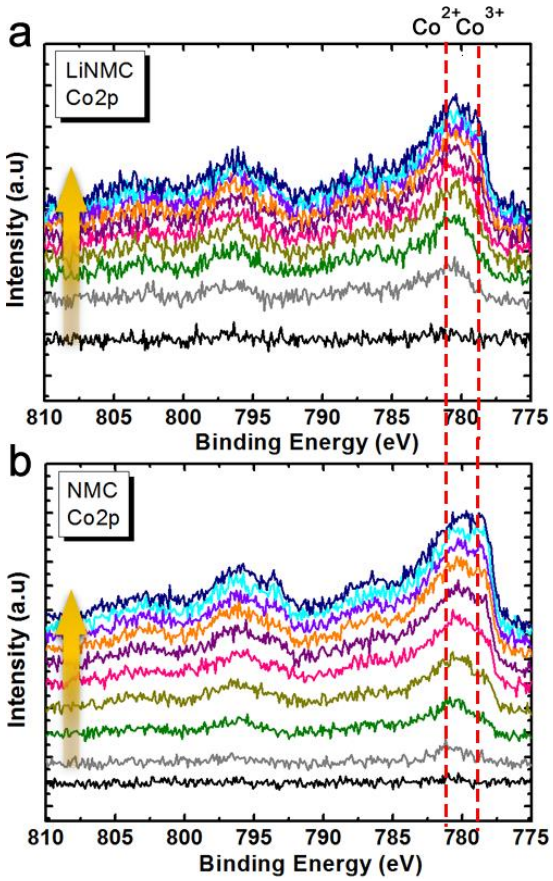

Figure S2. X-ray photoelectron spectroscopy Co $2p^{3/2}$ peaks of LiNMC and NMC anode materials at the end of first delithiation step. Dashed lines were added to help guide eye. The arrows point the direction of etching (i.e. towards the bulk of the sample).

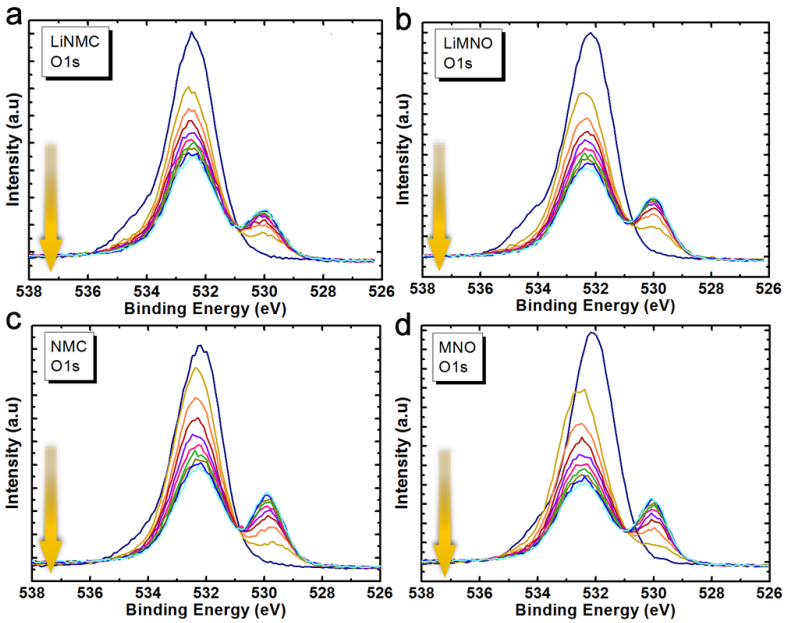

Figure S3. X-ray photoelectron spectroscopy O 1s peaks of four anode materials at the end of first delithiation step. Dashed lines were added to help guide eye. The arrows point the direction of etching (i.e. towards the bulk of the sample).

References

1. P. Poizot, S. Laruelle, S. Grugeon, L. Dupont, J.M. Tarascon, *Nature*, 407 (2000) 496
2. B. Varghese, M.V. Reddy, Z. Yanwu, C.S. Lit, T.C. Hoong, G.V.S. Rao, B.V.R. Chowdari, A. T. S. Wee, C.T. Lim, C.H. Sow, *Chem. Mater*., 20 (2008) 3360
3. L. Zhan, S. Wang, L.X. Ding, Z. Li, H. Wang, *Electrochim. Acta*, 135 (2014) 35
4. J. Yuan, X. Zhang, C. Chen, Y. Hao, R. Agrawal, C. Wang, W. Li, H. Yu, Y. Yu, X. Zhu, Z. Xiong, Y. Xie, *Mater. Lett.*, 190 (2017) 37
5. X. Sun, Y. Xu, P. Ding, M. Jia, G. Ceder, *J. Power Sources*, 244 (2013) 690
6. X. Gu, J. Yue, L. Li, H. Xue, J. Yang, X. Zhao, *Electrochim. Acta*, 184 (2015) 250
7. L. Li, L. Wang, X. Zhang, M. Xie, F. Wu, R. Chen, *ACS Appl. Mater. Interfaces*, 7 **(2015)** 21939
8. K.W. Nam, W.S. Yoon, X.Q. Yang, *J. Power Sources*, 189 (2009) 515
9. K.R. Chemelewski, E.S. Lee, W. Li, A. Manthiram, *Chem. Mater., 25 (2013) 2890*
10. M. Letiche, M. Hallot, M. Huve, T. Brousse, P. Roussel, C. Lethien, *Chem. Mater., 29 (2017) 6044*
11. M. Kunduraci, G.G. Amatucci, *J. Electrochem. Soc*., 153 (2006) A1345
12. W. Wei, Z. Wang, Z. Liu, Y. Liu, L. He, D. Chen, A. Umar, L. Guo, J. Li, *J. Power Sources*, 238 (2013) 376
13. M.Y. Cheng, Y.S. Ye, T.M. Chiu, C.J. Pan, B.J. Hwang, *J. Power Sources*, 253 (2014) 27
14. L. Leveau, B. Laik, J.P. Pereira-Ramos, A. Gohier, P. Tran-Van, C.S. Cojocaru, *J. Power Sources*, 316 (2016) 1
15. Z. Chen, J. Wang, D. Chao, T. Baikie, L. Bai, S. Chen, Y. Zhao, T. C. Sum, J. Lin, Z. Shen, *Scientific Reports*, 6 (2016) 25771
16. Z. Lu, Y. Liu, X. Lu, H. Wang, G. Yang, Y. Chao, W. Li, F. Yin, *J. Power Sources*, 360 (2017) 409
17. S. Kim, M. Kim, I. Choi, J. J. Kim, *J. Power Sources*, 336 (2016) 316
18. E. Jabry, G. Boissier, A. Rousset, R. Carnet, A. Lagrange, *J. Phys. Colloque*., 47 (1986) C1
19. A. Ramirez, P. Hillebrand, D. Stellmach, M. M. May, P. Bogdanoff, S. Fiechter, *J. Phys. Chem. C*, 118 (2014) 14073
20. S. Lee, K. Lee, K. Kim, M. Park, *Procedia Eng.*, 168 (2016) 1279
21. P. Balaya, A. J. Bhattacharyya, J. Jamnik, Y. F. Zhukovskii, E. A. Kotomin, J. Maier, *J. Power Sources*, 159 (2006) 171
22. J. S. McCloy, C. Leslie, T. Kaspar, W. Jiang, R. K. Bordia, *J. Appl. Physics*, 111 (2012) 07E1491
23. Z. Pu, H. Zhou, Y. Zheng, W. Huang, X. Li, *Appl. Surface Science*, 410 (2017) 14
24. S. Song, S. Yao, J. Cao, L. Di, G. Wu, N. Guan, L. Li, *Appl. Catalysis B*, 217 (2017) 115
25. T.G.U. Ghobadi, M. Kunduraci, E. Yilmaz, *J. Alloys Comp.*, 730 (2018) 96
26. R. Jin, Y. Meng, Y. Ma, H. Li, Y. Sun, G. Chen, *Electrochim. Acta*, 209 (2016) 163
27. K. Wang, Y. Huang, M. Wang, M. Yu, Y. Zhu, J. Wu, *Carbon*, 125 (2017) 375
28. J. Xu, L. He, W. Xu, H. Tang, H. Liu, T. Han, C. Zhang, Y. Zhang, *Electrochim. Acta*, 145 (2014) 185
29. L.X. Zhang, Y.L. Wang, H.F. Jiu, W.H. Zheng, J.X. Chang, G.F. He, *Electrochim. Acta*, 182 (2015) 550
30. X. Pan, J. Ma, R. Yuan, X. Yang, *Mater. Chem. Phys*., 194 (2017) 137